

H.J. Bray · S.A.T. Redfern

Kinetics of dehydration of Ca-montmorillonite

Received: 28 August 1998 / Revised, accepted: 27 January 1999

Abstract Isothermal thermogravimetric experiments have been carried out to determine the reaction kinetics of the dehydration processes in fuller's earth, a natural Ca-montmorillonite. Dehydration in swelling clays is a complex reaction, and analysis of the thermogravimetric data using empirical rate equations and time-transformation analysis reveals that the nature of the rate controlling mechanism is dependent upon both the temperature regime of the sample as well as the extent of reaction. For fuller's earth, we find that the dehydration kinetics are dominated by a nucleation and growth mechanism at low temperatures and fractions transformed (stage I), but above 90 °C the last stages of the reaction are diffusion controlled (stage II). The activation energy for dehydration during stage I is around 35 kJ · mol⁻¹, whereas the removal of water during stage II requires an activation energy of around 50 kJ · mol⁻¹. These two stages of dehydration are associated with primary collapse of the interlayer (stage I) and movement of water that is hydrated to cations within the interlayer (stage II).

Key words Montmorillonite · Fuller's earth · Dehydration · Kinetics · Thermogravimetry

Introduction

The high-temperature dehydration transformations of fuller's earth are of great importance in ceramic technology, since this and other related clays are typically major components of commercial clay bodies. Temperatures encountered during the production of fired ceramics can reach as high as 1100 °C, and the drying process of the clay beforehand greatly affects the phases formed on firing. In addition, this natural material finds

important uses as a physical seal and chemical absorbent in chemical and nuclear waste management. In this context it is important to understand the characteristics and controlling reaction mechanism of high-temperature transformations in these swelling clays.

Fuller's earth is the term used to describe a Ca-montmorillonite with significant swelling capacities. The structure comprises a dioctahedral 2:1 layer, readily taking up water and organic molecules between the aluminosilicate sheets. Substitution in the central octahedral sheet (Fe²⁺ and/or Mg²⁺ for Al³⁺) and the outer tetrahedral sheet (Al³⁺ for Si⁴⁺) causes a negative charge on the outer basal oxygens. Interlayer cations balance this charge, forming hydration spheres and (together with interlayer molecular H₂O) force the crystalline layers apart. Dehydration involves the removal of interlayer water up to 350 °C, followed (at higher temperatures) by dehydroxylation as water molecules are formed from hydroxyls in the octahedral sheet.

The hydration and dehydration reactions of montmorillonite are important in many geological processes and have been linked to phenomena as diverse as sediment overpressuring (Powers 1967; Barker 1972; Magara 1975; Plumley 1980; Bruce 1984), the migration of petroleum (Powers 1967; Burst 1969), listric faulting (Bruce 1984) and the well-known smectite to illite transition (Powers 1967; Perry and Hower 1972; Weaver and Beck 1971; Hower et al. 1976; Freed and Peacor 1989; Pytte and Reynolds 1988; Velde and Vasseur 1992; Ransom and Helgeson 1995).

The temperatures and characteristics of dehydration reactions in the swelling clays provide important information about the interlayer configuration, since the dehydration process depends on the composition of the counterbalancing cations in the interlayer and charge on the tetrahedral sheet. Experimental studies by Koster van Groos and Guggenheim (1984, 1986, 1987) have demonstrated that montmorillonite dehydrates in two stages. The two dehydration steps were interpreted as dehydration of voluminous, but weakly bonded, water

H.J. Bray · S.A.T. Redfern (✉)
Department of Earth Sciences, University of Cambridge,
Downing Street, Cambridge, CB2 3EQ, UK

from the outer hydration shell of the interlayer cation, followed by dehydration of water from a more strongly-bonded inner hydration shell environment. It is well known that dehydration depends on interlayer cation chemistry. For example, the radius, charge and hydration energy of counterions can control dehydration temperatures. Dehydration may also be influenced by other factors, for example the location of the layer-charge and the clay particle size (Annabli-Bergaya et al. 1996).

The kinetics of the smectite to illite transition have been investigated extensively in earlier studies, with the estimated activation energy lying between $12.6 \text{ kJ} \cdot \text{mol}^{-1}$ and $125.6 \text{ kJ} \cdot \text{mol}^{-1}$ (Eberl and Hower 1976; Robertson and Lahann 1981; Howard and Roy 1985; Huang et al. 1994). There have been fewer attempts to probe thoroughly the kinetics of dehydration of montmorillonites. Girgis et al. (1986) conducted non-isothermal experiments on a series of naturally occurring predominantly Ca-smectites, they concluded that dehydration follows a first order reaction with values ranging from $39.8 \text{ kJ} \cdot \text{mol}^{-1}$ to $52.3 \text{ kJ} \cdot \text{mol}^{-1}$. No discrimination was made between interlayer water that was physically adsorbed and water attached in hydration shells of the exchangeable cations. Furthermore, Güler and Sarier (1990) calculated a value of $14.72 \text{ kJ} \cdot \text{mol}^{-1}$, assuming that a first order reaction occurs, following the work of Murray and White (1949, 1955a, b, c, d). However, it should be noted that Murray and White studied dehydroxylation, rather than interlayer dehydration. Waclawska (1984) described a zero-stage process with activation energies ranging from 15.1 to $26.4 \text{ kJ} \cdot \text{mol}^{-1}$, but failed to provide any details of the physical nature of the dominating reaction mechanism.

More recently, computer simulations of the molecular structure of water and the distribution of the counterions in the interlayer region have extended our understanding of the structure of these clays (Chang et al. 1995; Skipper et al. 1989, 1991, 1995a, b; Bridgeman et al. 1996; Karaborni et al. 1996). Good agreement was found between the enthalpies of swelling clays determined from Monte Carlo and molecular dynamic simulations (De Siqueira et al. 1997) and enthalpies derived from experimental thermodynamic data (Greene-Kelly 1955; Low, 1979; Moore and Hower 1986; Huang et al. 1994; Wu et al. 1997). These simulations also indicate that the interlayer water structure deviates significantly from the structure of bulk liquid water, showing ordering akin to that of a smectic liquid crystal, but then becoming increasingly disordered with increasing interlayer water and interlayer repeat. The degree of hydration and the location of charge deficiency depends upon the distribution of the interlayer cations within the tetrahedral and octahedral sheets of the 2:1 layer structure. The simulations confirm the earlier findings of Farmer and Russell (1967), that negative charge in the tetrahedral sheet due to the substitution of Al^{3+} for Si^{4+} is localised on the three surface oxygens attached to the Al^{3+} substituent. Negative charge arising from

octahedral substitution (Mg^{2+} and/or Fe^{2+} for Al^{3+}), is more diffusely spread over the surface oxygens.

Finally, the end of dehydration is accompanied by collapse of the interlayer region, but the 2:1 tetrahedral:octahedral sheets remain intact. At this stage, the interlayer cation is thought to either reside in the ditrigonal cavities of the outer tetrahedral sheet or migrate into the octahedral sheets (Heller-Kallai and Rozenson 1980).

Many kinetic studies assume that the dominating reaction processes is a single rate-controlling process throughout all stages of the reaction. Furthermore, it is often accepted that the associated activation energy remains constant throughout the transition. This investigation seeks to test these assumptions, and shows how the rate-controlling process changes throughout the reaction and the temperature regime chosen. The 'time to' method of kinetic analysis of isothermal data, described by Burke (1965), has been employed in order to test the validity of these assumptions and determine any variations in the energetics of the reaction.

Experimental procedures

The sample selected for study was a naturally occurring Ca-montmorillonite from Redhill, UK, kindly provided by Dr. S. Drachman of RBB Ltd. X-ray diffraction of the sample revealed it to be a smectite-rich clay with an initial 001 *d*-spacing of approximately 15 \AA . The structural formula of the $< 2 \mu\text{m}$ fraction was determined as $\text{Ca}_{0.59}\text{K}_{0.38}\text{Na}_{0.13}(\text{Si}_{7.72}\text{Al}_{0.28})(\text{Al}_{2.71}\text{Fe}_{0.50}^{2+}\text{Mg}_{0.57}\text{Ti}_{0.08})\text{O}_{20}(\text{OH})_4$ by X-ray fluorescence spectroscopy.

The sample was initially ground by hand in a pestle and mortar and dry sieved below $53 \mu\text{m}$, to further purify the clay fraction. Preliminary mass loss and differential scanning calorimetry (DSC) were carried out on a loosely packed sample placed in a platinum crucible in an atmosphere of air. A Netzsch STA 409 simultaneous thermal analysis instrument was used, employing alumina as a reference. The data were obtained at a constant heating rate of $10 \text{ }^\circ\text{C}/\text{min}$, giving clear DSC data that can be correlated to mass loss events collected from the thermobalance (Fig. 1).

The $< 2 \mu\text{m}$ fraction was separated following a method similar to that of Tang and Sparks (1993): 50 g of clay was dispersed in 2 l

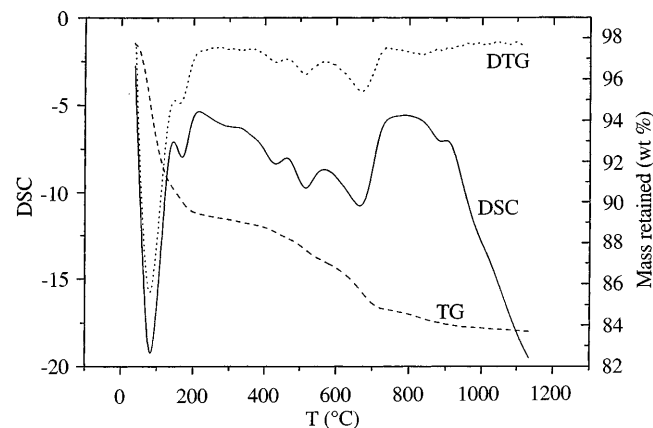


Fig. 1 Preliminary thermal analysis, TG and DSC experiment at $10 \text{ }^\circ\text{C}/\text{min}$, for the $< 53 \mu\text{m}$ fraction of fuller's earth (Ca-montmorillonite)

of water for 24 h. The clay was then left to settle out, and the upper portion syphoned off to collect the fraction below 2 μm as determined by Stoke's law. The clay solution was then centrifuged for one hour at 2500 rpm, and the supernatant fluid was decanted off. Finally, the clay fraction was freeze-dried.

The kinetics of dehydration were investigated by isothermal mass loss experiments carried out using a Stanton Redcroft TG 761 thermobalance. The atmosphere could be controlled by a constant flow of dry nitrogen. The starting mass of all samples was between 9.9 and 10.1 mg to ensure there were no spurious effects due to the build up of local vapour pressure. The mass loss experiments were carried out for one hour each, between room temperature and 150 $^{\circ}\text{C}$.

Results

Preliminary thermal analysis (TG and DSC) at 10 $^{\circ}\text{C}/\text{min}$ indicate there are many stages of mass loss in the temperature range of 25–1000 $^{\circ}\text{C}$ (Fig. 1). Interlayer water loss dominates the behaviour below 350 $^{\circ}\text{C}$. An initial rapid mass loss (up to 150 $^{\circ}\text{C}$) is followed by slower mass loss approaching a constant value towards the end of dehydration. The reaction appears to occur in two stages, revealed by two endotherms observed in the DSC experiments. A total mass loss of over 10 wt.% can be assigned to the dehydration of interlayer water.

Further mass loss, after the removal of interlayer water, occurs at higher temperatures (430–665 $^{\circ}\text{C}$), the region over which dehydroxylation becomes important. Hydroxyls combine in the central octahedral sheet to form water molecules. The reaction appears to proceed over a wide range of temperatures and three endotherms are observed in the DSC run. These occur at 430, 520 and 665 $^{\circ}\text{C}$, the two higher temperature endotherms representing the main dehydroxylation events. A mass loss of 2 wt.% is observed for each of these reactions. At very high temperatures, at around 800 $^{\circ}\text{C}$, there appears to be a slight mass loss (of around 1 wt.%) and a broad exotherm. A constant mass loss is observed above 925 $^{\circ}\text{C}$, at which temperature a further sharper exotherm is seen.

Isothermal mass loss experiments (20–150 $^{\circ}\text{C}$) for the dehydration reaction (Fig. 2) show a rapid mass loss in

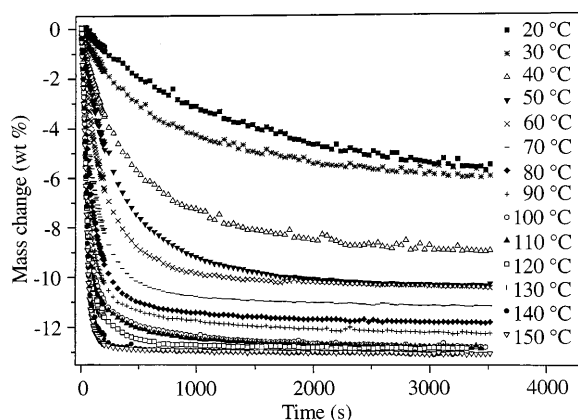


Fig. 2 Isothermal mass change against time for fuller's earth, collected from 20 $^{\circ}\text{C}$ to 150 $^{\circ}\text{C}$

the first 500 seconds of heating, followed by a period of slower more constant mass loss. A room temperature experiment was performed to show the effect of constant nitrogen gas flow on water loss: a value of around 4 wt.% can be attributed to humidity-dependent dehydration due to the dry nitrogen atmosphere. The lowest temperature runs showed the smallest mass loss at the end of the hour long experiment: they retain a greater amount of water than the samples run at higher temperatures. It seems that, up to a temperature of 100 $^{\circ}\text{C}$, the mass of the sample at the end point of the reaction decreases with increasing temperature. Above this temperature the percentage mass lost at the end point of each isothermal run was identical to within 0.2 wt.%.

Kinetic analysis

The thermal transformations for Ca-montmorillonite appear complex, reflected by the many endotherms recorded by DSC (Fig. 1). The dehydration rate is rapid, and can begin before the target temperature has been reached in the furnace (Fig. 2). It can be seen from the mass change versus time curves that complete dehydration was not attained in the experiments. Equilibration to a constant mass occurred at each temperature, even though the atmosphere was a constant dry nitrogen purge, and this constant mass implies finite H_2O contents remain after long time intervals. This behaviour could indicate that a local H_2O vapour pressure is set up in the sample, and that the gas purge was not effective in removing the complete H_2O layer (Line et al. 1995). On the other hand, it seems more likely that the clay has reached a stable water content as a function of the conditions of the sample.

The final mass reached at each temperature is dependent on the amount of sample and the manner of packing of the sample into the platinum crucible. As the initial sample mass was kept constant between 9.9–10.1 mg, effects due to packing must be responsible for difference in the final mass change observed. To eliminate any effects due to the random packing of the sample, for each individual temperature the experiment was repeated four times to ensure a reproducible and reliable data set. It is important to note that even though the final mass change shown by the sample was sometimes anomalous, the rate of mass change as a function of time remains unchanged for each data set. This shows that the TG technique is a reliable method for measuring the rate of reaction, as a function of time at a specific temperature.

To determine the reaction coordinate, or fraction transformed (α), one has to know the end point of the reaction (the state corresponding to $\alpha = 1.0$). A simple first-order exponential function was fitted to the data for times greater than 1000 s, so the data could be expressed in terms of α . The fraction transformed was then accurately determined, as a function of time for each isothermal experiment (Fig. 3). The lower temperature

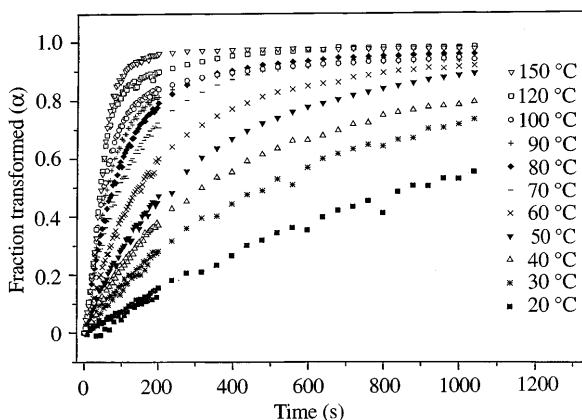


Fig. 3 Time evolution of the fraction transformed (α), calculated from the mass change as a function of time

experiments did not always go to completion, and clearly react at a slower rate.

In order gain some insight into the reaction mechanism on an atomic scale, attempts were made to fit the data to a series of solid-state rate equations. A well-established method of data analysis assumes the general rate Eq. (1), which expresses the rate of the reaction as a product of a function of the fraction transformed (α) and a rate constant (k):

$$\frac{d\alpha}{dt} = kf(\alpha) \quad (1)$$

which can be expressed in integrated form as

$$g(\alpha) = kt \quad (2)$$

The function $g(\alpha)$ is dependent on the mechanism of the reaction, and this dependence is often used to infer an atomic reaction mechanism.

Sharp et al. (1966) have shown that reduced time scale plots facilitate the comparison of experimental data. Isokinetic data from a number of experimental runs should line on a single curve. This curve can then be compared to that expected for any one of a number of different theoretical rate equations (Table 1). The rate equations can be divided into three general groups: (1) phase-boundary and first order reactions, (2) diffusion controlled reactions, (3) reactions described by the Avrami equation (Avrami, 1939).

Table 1 Integrated rate equations, showing the corresponding calculated values of the exponent m for the Avrami and Austin-Rickett empirical rate laws

Mechanism	Function $g(\alpha)$	Slope (m)	Slope (m_A)
Zero order	α	1.17	1.36
R2 – phase boundary reaction, cylindrical	$1 - (1 - \alpha)^{1/2}$	1.10	1.31
R3 – phase boundary reaction, spherical	$1 - (1 - \alpha)^{1/3}$	1.06	1.27
F1 – random nucleation, one nucleus/particle	$-\ln(1 - \alpha)$	1.00	1.19
A2 – random nucleation, Avrami equation I	$[-\ln(1 - \alpha)]^{1/2}$	2.00	2.39
A3 – random nucleation, Avrami equation II	$[-\ln(1 - \alpha)]^{1/3}$	3.00	3.58
D1 – one-dimensional diffusion	α^2	0.60	0.72
D2 – two-dimensional diffusion, cylindrical	$(1 - \alpha) \ln(1 - \alpha) + \alpha$	0.57	0.67
D3 – three-dimensional diffusion, spherical	$[1 - (1 - \alpha)^{1/3}]^2$	0.53	0.63
D4 – three-dimensional diffusion, spherical, Ginstling-Broughtein	$(1 - \frac{2}{3}\alpha) - (1 - \alpha)^{2/3}$	0.55	0.66

The reduced time plots shown in Fig. 4 use $t/t_{0.3}$ to test for the reaction mechanism involved. Frequently, $t/t_{0.66}$ has been employed, but by scaling the time dependent behaviour to that at 30% of the reaction one is better able to discriminate differences at higher values of α (Mohamed and Sharp 1997). It can be seen that our experimental data is not isokinetic between 20 °C and 150 °C: the reaction cannot be described by a single rate equation over the entire temperature range. The experiment at 50 °C lies between a first order reaction and a diffusion controlled reaction. At 100 °C the initial reaction appears to be dominated by a phase-boundary mechanism, and at 150 °C the initial reaction could be described by the Avrami equation. Therefore, on increasing temperature the rate-determining step appears to be changing, and there is evidence that the reaction could be multistage, or at least a mixture of two reaction mechanisms.

Empirical rate equations

Rather than fitting the data to one of a number of possible rate equations, and attempting to discern the rate controlling process by judging the goodness of fit

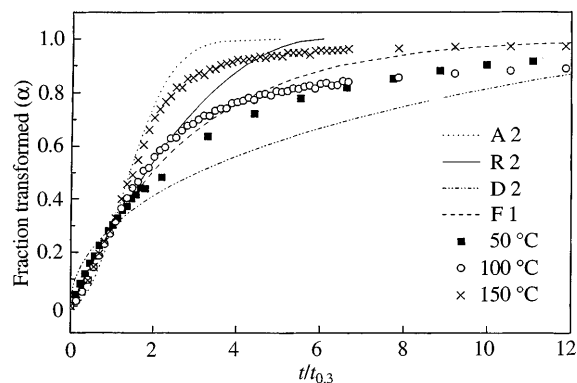


Fig. 4 Reduced time plots ($t/t_{0.3}$) for the dehydration reaction of Ca-montmorillonite at 50, 100 and 150 °C. The expected evolutions of the fraction transformed for random nucleation (A2), phase boundary (R2), diffusion (D2) and nucleation (F1) controlled reactions are shown by the lines. The data for Ca-montmorillonite dehydration to lie between a mixture of processes at low temperature, changing in character with temperature and fraction transformed (α)

between the data and each rate equation, it is possible to employ a general rate equation in which the function, $f(\alpha)$, (in Eq. 1) is expressed in some general manner with a variable parameter that reflects the rate controlling mechanism. Such rate equations are sometimes termed “empirical rate equations”. Two such equations are commonly used, that developed by Avrami (1939) and that developed by Austin and Rickett (1939). We have used each of these to analyse our data for smectite dehydration. The Johnson-Mehl or Avrami method expresses the general rate Eq. (1) such that the rate constant (k) and the controlling reaction mechanism (related to a parameter, m) can be determined simultaneously (Hancock and Sharp 1972):

$$\frac{d\alpha}{dt} = k^m \cdot t^{m-1} (1 - \alpha) \quad (3)$$

Following integration of Eq. (3), the fraction transformed can be written as the linearised form of the Avrami equation:

$$\ln(-\ln(1 - \alpha)) = m \ln k + m \ln t \quad (4)$$

The values of k and m can be calculated from the intercept and gradient of a ‘lnln’ plot of the data. If a single reaction mechanism operates through the temperature range and several data sets are isokinetic, they will plot as a set of parallel lines with a constant value of m . Values of m (in Eq. 4) for a range of established rate equations were first presented by Hancock and Sharp (1972). We have recalculated these for $0.15 < \alpha < 0.5$ for both the Avrami equation and for the Austin-Rickett equation (Table 1).

Our data for $0.1 \leq \alpha \leq 0.9$ are shown as an Avrami ‘lnln’ plot in Fig. 5a. The gradient m increases with temperature, and at higher temperatures, is also a function of the fraction transformed, α (Table 2). There appear to be three different temperature regimes.

Firstly, from 20 to 80 °C, the reaction appears isokinetic, with a single dominant rate-limiting step. The average gradient, m , over this temperature range is 0.84. This value does not correspond to any one of the nine rate equations shown in Table 1. Rather, it is intermediate between the value expected for a first order reaction and that expected for diffusion control. It seems likely, therefore, that the reaction is first order at these temperatures, slowed down by the diffusional control of the movement of molecular water from the interlayer space.

Secondly, between 80 and 130 °C, there appears to be a change in behaviour. The Avrami plots show a more pronounced negative curvature and there appears to be more than one linear section. Criado et al. (1984), Goss (1987) and Ruan and Gilkes (1996) found (in other systems) that ‘lnln’ plots may often be split into several linear sections, indicating that several reaction processes are operating, their relative influence on the kinetics of the reaction changing as a function of α . Very rapid changes are still observed at the early stages of the reaction, as well as an increase in m with temperature. Towards the end of the reaction, in isothermal runs at

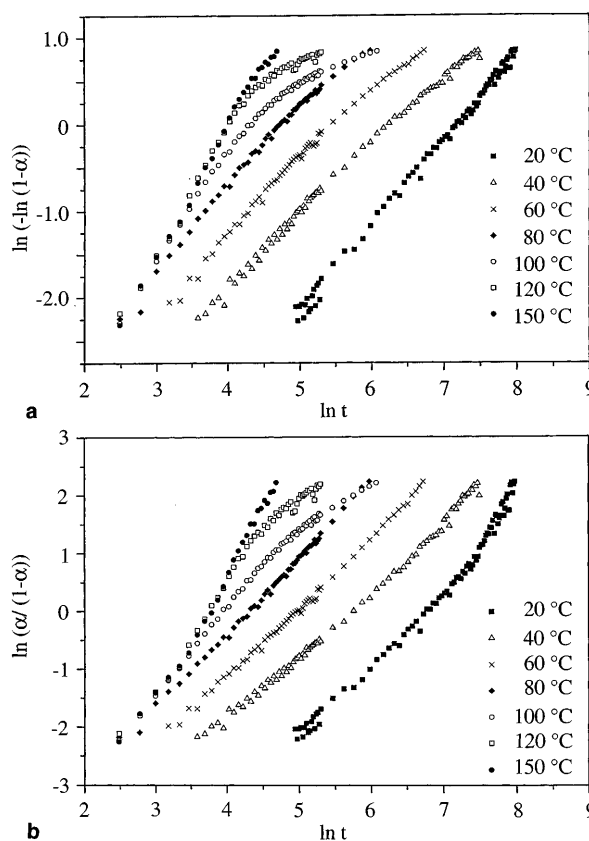


Fig. 5 **a** Avrami ‘lnln’ plot and **b** Austin-Rickett plot, for $0.1 < \alpha < 0.9$. Deviations from linearity are observed towards the end of the reaction at higher temperatures

these temperatures, a second stage in the reaction becomes apparent (Table 2). The initial rate limiting process (with $m = 1.20$) could be the advancement of a phase boundary. At higher values of α (>0.70), the gradient changes ($m = 0.41$). Therefore, we conclude that during dehydration at these temperatures the rate-controlling mechanism changes from first-order to diffusion controlled. The initial water loss is very rapid, and the first-order control is most likely associated with a strain-related interface, as the interlayer space collapses upon dehydration of the first layer of water lost. The water removed during the second stage is more firmly held (probably in the hydration sphere around the interlayer cation) and is involved in water-cation interactions. This water does not start to leave the structure until dehydration of the first type is complete. The diffusion of this more firmly held water is therefore the rate determining step during the final stages of the dehydration process.

Finally, at the highest temperatures (140 °C and 150 °C), the ‘lnln’ plots once more show only one linear section (Fig. 5a). It is likely that this is because of the very rapid reaction of the sample, which begins even as the sample starts to heat up within the apparatus, but before it has reached the set soak temperature. The system is far from equilibrium upon heating to such high

Table 2 Values of the rate constant (k) and exponent (m) for the first and second stages of dehydration of fuller's earth determined using the Avrami method and Austin-Rickett method

T °C	Avrami		Austin-Rickett		
	k	m	k	m	m
Stage I					
20	0.00080(4)	0.9940(7)	0.00010(9)		1.37(2)
30	0.0033(3)	0.859(6)	0.00077(6)		1.19(1)
40	0.0069(3)	0.786(6)	0.00157(8)		1.137(8)
50	0.0068(2)	0.844(6)	0.0015(1)		1.21(1)
60	0.0112(7)	0.81(1)	0.0027(1)		1.194(8)
70	0.0120(5)	0.834(8)	0.0050(3)		1.18(7)
80	0.0104(6)	0.96(1)	0.00372(3)		1.30(4)
90	0.0085(6)	1.06(2)	0.0043(2)		1.32(8)
100	0.0056(4)	1.20(2)	0.0030(2)		1.46(1)
110	0.0042(4)	1.31(2)	0.0015(1)		1.68(2)
120	0.0027(2)	1.47(3)	0.00099(7)		1.85(3)
130	0.0035(4)	1.42(3)	0.0014(2)		1.79(3)
140	0.0026(3)	1.45(3)	0.00035(5)		2.12(4)
150	0.0025(2)	1.48(2)	0.00035(6)		2.15(5)
T °C	Avrami		Austin-Rickett		
	α	k	α	k	m
Stage II					
80	0.78	0.058(9)			
90	0.70	0.13(1)	0.8	0.04(1)	0.87(5)
100	0.70	0.21(2)	0.8	0.09(1)	0.76(2)
110	0.76	0.31(2)	0.8	0.14(2)	0.71(3)
120	0.73	0.25(3)	0.84	0.13(8)	0.80(9)
130	0.75	0.14(2)			

temperatures, and this is reflected in the increased value of the gradient ($m = 1.5$). The driving force for the reaction is high, and no information about the second stage of reaction can be extracted because the reaction runs to exhaustion by a first-order mechanism before reaching the second stage seen at lower temperatures.

Two reaction stages are recorded in the Avrami 'lnln' plots. The specific point at which the gradient changes could be affected by the slight negative curvature observed in the higher temperature Avrami 'lnln' plots. If the Avrami 'lnln' plot show a slight negative curvature it is often useful to replace $(1-\alpha)$ in Eq. (3) with $(1-\alpha)^2$ (Burke 1965), and the empirical rate equation becomes equivalent to that of Austin and Rickett (1939):

$$\frac{d\alpha}{dt} = k^{m_A} \cdot t^{m_A-1} (1-\alpha)^2 \quad (5)$$

or, in linearised integrated form:

$$\ln\left(\frac{\alpha}{1-\alpha}\right) = m_A \ln k_A + m_A \ln t \quad (6)$$

This defines another exponent m_A and rate constant k_A , which differ from m and k in the Avrami equation.

Analysis of the data using Eq. (6) (rather than Eq. 4) confirms the results of the Avrami analysis for the data below 80 °C (dominantly first order with nucleation and growth of a reaction front controlling the initial stage of dehydration) and above 130 °C. At intermediate temperatures the gradient m_A increases with temperature in the same way as has been seen in the Avrami 'lnln' plots. Figure 5a, b shows the Avrami and Austin-Rickett plots

respectively. At intermediate temperatures, the latter can be split into two separate linear sections. The second linear section occurs for $\alpha > 0.8$, with an average value of $m_A = 0.79$ (Table 2). The break in slope in the Austin-Rickett plots occurs at a higher α than when plotted according to Eq. (4). This is because this method removes the negative curvature seen in the Avrami plots, and better differentiates the two linear sections. The values of m_A determined for the second stage suggest a diffusion controlled process, confirming the conclusions from the Avrami 'lnln' plots. It is very difficult to differentiate between the different diffusion-controlled rate equations (Table 1). Considering the structure of montmorillonite, a two dimensional diffusion mechanism is expected, corresponding to movement of water parallel to (001).

Determination of the activation energy (E_a)

From rate constants, k

We have determined values of rate constant, k , for the Avrami equation and k_A for the Austin-Rickett equation for isothermal runs between 20 °C and 150 °C (Table 2). An estimate of the activation energy (E_a) can be obtained using the Arrhenius equation, $k = A \exp(-E_a/RT)$.

As the data in the lowest temperature regime were found to be isokinetic, those from the region from 30–80 °C have been used to determine the energetics for the first stage of the dehydration process (Fig. 6). In addi-

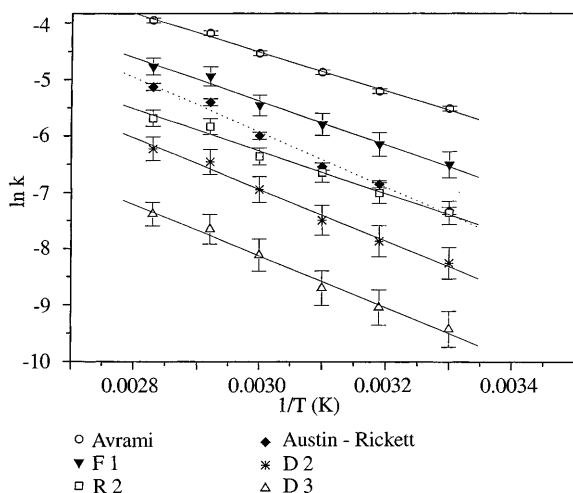


Fig. 6 Arrhenius plot of $\ln k$ against $1/T$ (K) for the initial stage of dehydration, determined from the integrated rate equations, Eq. 7, and both the Avrami and Austin-Rickett rate laws

tion to using the empirical rate equations to determine the temperature dependence of k , we have followed the work of Miletich et al. (1997) to accurately calculate the reaction rate k for each individual temperature run. The mass change versus time data was fitted by a least squares procedure to a simple exponential function

$$m_t = m_{eqm} + \Delta m \cdot e^{-\{k(t-t_0)\}^n} \quad (7)$$

where m_t is initial mass at time t , m_{eqm} is the mass at $t = \infty$, and $\Delta m = m_o - m_{eqm}$. The exponent n was fixed at 0.84, in accordance with the value implied by the Avrami equation. Using, therefore, values of k obtained at each temperature Eqs. (4), (6), and (7), we have obtained three possible values for the activation energy of dehydration. These three methods of calculating activation energies render values of $28.6 \pm 0.9 \text{ kJ} \cdot \text{mol}^{-1}$ (Avrami method), $34.2 \text{ kJ} \cdot \text{mol}^{-1}$ (Eq. 7), and a higher value of $40.6 \pm 2.2 \text{ kJ} \cdot \text{mol}^{-1}$ from the Austin-Rickett equation (Table 3).

Table 3 Activation energies (E_a), for the first stage of dehydration, calculated from the rate equations in Table 1, by fitting the data to Eq. 7, and by both the Avrami and Austin-Rickett methods

Rate equation	Activation Energy ($\text{kJ} \cdot \text{mol}^{-1}$)
Avrami	28.6 ± 0.9
Austin-Rickett	40.5 ± 2.2
Gualtieri et al. (1995)	35.4 ± 1.6
First order	32.3 ± 1.9
R2	31.3 ± 2.2
R3	31.6 ± 2.1
D1	37.5 ± 2.1
D2	38.1 ± 2.0
D3	38.0 ± 1.9
D4	38.4 ± 2.0
Miletich et al. (1997)	34.2 ± 1.6
Average	35.5 ± 0.5

Values of rate constant (k) can also be calculated using the integrated rate equations in Table 1. First order, phase boundary and diffusion rate equations were used (whether they were deemed physically appropriate or not) to calculate an activation energy. An average value of $35.5 \pm 0.5 \text{ kJ} \cdot \text{mol}^{-1}$ was obtained (Table 3). Gualtieri et al. (1995) employed a rate equation based on instantaneous nucleation and growth model (first order), but with an experimental coefficient related to diffusion, which contributes to a decrease in the reaction rate ($0.75[-\ln(1-\alpha)^{4/3}] = kt$). Using this rate equation we obtain an activation energy of $35.4 \text{ kJ} \cdot \text{mol}^{-1}$, which is in agreement with the average value from all the rate equations and the value obtained using Eq. (7). The spread of activation energies obtained using this diverse suite of rate equations is quite small. The phase boundary and first order rate laws tend to give lower values of the activation energy, whilst the diffusion controlled rate laws give values higher than the average. The values calculated from Eq. 7 and from Gualtieri et al.'s (1995) rate equation both lie close to the average.

The activation energy for the second stage of the reaction is more difficult to calculate by this method, as this subsequent diffusion controlled reaction was only observed across a small temperature and α regime. It is therefore difficult to resolve accurate values of the intercept in Avrami or Austin-Rickett plots, since this is strongly dependent on choice of starting point for the second stage of the reaction at each temperature. In fact, the values of k quoted for stage II of the dehydration reaction in Table 2 do not seem to describe the rates of reaction implied by the raw data.

Using the “time to a given fraction” method

A potential pitfall of the method described is the assumption that activation energy (E_a) remains constant throughout the reaction process, and is correctly determined from the rate laws. The Avrami and Austin-Rickett plots have already indicated that, at lower temperatures, the reaction is probably dominated by a combination of two processes. In addition, at higher temperatures (80–120 °C), the dominant mechanism appears to change through the reaction, and therefore likely there is a change in activation energy as the reaction proceeds. Redfern (1987) suggested that the activation energy must be determined independently of the empirical function $g(\alpha)$, if any change in activation energy is to be observed. This is often referred to as the “time to a given fraction” method, and relies on the fact that the fraction transformed (α) and the time t are functionally related. The time t can be made the dependent variable by rewriting Eq. (1):

$$dt = k^{-1} f^{-1}(\alpha) d\alpha \quad (8)$$

The time t_Y to transform a given fraction Y is then

$$t_Y = k^{-1} \int_{\alpha=0}^{\alpha=Y} f^{-1}(\alpha) d\alpha \quad (9)$$

and if the function $f^{-1}(\alpha)$ does not change over the temperature range studied the integral has a constant numeric value. Therefore $t_Y \propto k^{-1}$ or $t_Y \propto A^{-1} \exp(E_a/RT)$. Thus t_Y for a certain fraction transformed can be determined from the set of isothermal experiments, using $\ln t_Y = \text{const} - \ln A + E_a/RT$. A plot of $\ln t_Y$ against $1/T$ is linear if the activation energy does not change within the range of Y chosen.

The data for $20 < T < 80$ °C reveal a linear dependence at all values of fraction transformed between $\alpha = 0.1$ and $\alpha = 0.9$, giving an average activation energy, E_a , of 34.7 ± 0.9 kJ · mol⁻¹ (Fig. 7a). At $T > 90$ °C, the plots starts to tend towards horizontal at lower values of α . This is due to the fact that the sample is reacting before reaching the isothermal soak temperature for that experiment, so that small fractions of transformation occur at temperatures lower than the notional set temperature as the sample heats in the apparatus. Only on reaching higher fractions transformed is there some differentiation between the times required to reach certain points in the reaction. This effect is particularly pronounced above 130 °C where the samples reach all given fractions transformed at an identical

time (hence lines are horizontal): the sample has dehydrated fully during heating to the isothermal soak temperature. Furthermore, between 100 and 130 °C the activation energy increases with fraction transformed at values of $\alpha > 0.8$: this represents the second stage of the dehydration process, only seen at these temperatures and fractions transformed.

Previously, it was noted that the reaction changes above values of $\alpha > 0.8$ at these temperatures, therefore we have attempted to determine the energetics of the last stage of dehydration. Fig. 7b shows a \ln "time to a given fraction" plot, for $0.8 < \alpha < 0.9$, from which the activation energy is found to rise to a value of 47 ± 6 kJ · mol⁻¹.

Conclusions

The dehydration of Ca-montmorillonite is clearly a complex reaction, occurring rapidly under the conditions of this investigation. From the DSC measurements two endotherms are observed below 300 °C. The presence of two such endotherms is predominantly due to the hydration of calcium in the interlayer, since this results in the process of interlayer water removal occurring several stages (Waclawska 1984).

Thermogravimetry shows that, as the sample equilibrates over a range of isothermal temperatures, the end point of dehydration (shown by the total mass loss) is a function of temperature. It is essential to recognise this if an accurate kinetic analysis is to be carried out for the first stage of dehydration, since the data must be normalised against the expected end point for each temperature. When this is done, the reduced time plots ($t/t_{0.3}$) show that, at 50 °C, the dehydration reaction follows a kinetic path that lies between the curves calculated for diffusion (D2) and random nucleation (F1) controlled reactions. The Avrami plots ranging from 20 to 80 °C, reinforce this observation, indicating that the reaction control is intermediate between nucleation and growth process and diffusion. The Austin-Rickett (1939) method implies the dominating reaction mechanism is first order in nature, but this probably reflects that fact that this method over-corrects for a negative curvature in the 'lnln' plots, not observed in the original Avrami plots.

In conclusion, the rate-limiting step for the first stage of dehydration is well described by the nucleation and growth of a reaction front, which is slightly impeded by the strong electric fields of the Ca²⁺. The powerful hydrating properties of the interlayer cations are able to slightly hinder the migration of the water molecules from their outer hydration spheres.

It is observed that at higher temperatures (above 90 °C) the reaction is no longer isokinetic as a function of temperature: both the m and m_A values (in the Avrami and Austin-Rickett plots, respectively) increase with temperature. This is because the sample is far from equilibrium at the start of the isothermal shock heating

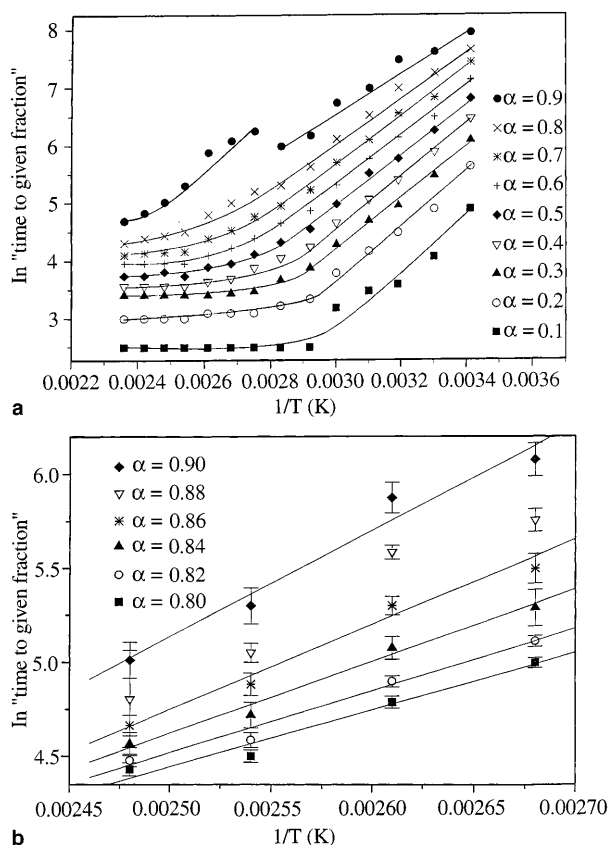


Fig. 7 a \ln "time to a given fraction" for $0.1 < \alpha < 0.9$, b for the second stage of the reaction ($0.8 < \alpha < 0.9$, $100 < T < 130$ °C)

experiment. We can not infer that the nature of water release is changing, this trend being recognised in both methods.

The second stage of the reaction process is observed towards the end of the reaction at high temperatures, at $\alpha > 0.7$ and $\alpha > 0.8$ for the Avrami and Austin-Rickett methods, respectively. A change in gradient of the 'lnln' plots is observed, suggesting that this second stage of the dehydration reaction is diffusion controlled, and could be linked to the removal of water from a different environment. The separation of the two stages is better seen using the Austin-Rickett method, and occurs at $\alpha > 0.8$.

Previous in situ X-ray synchrotron work on the dehydration of the same fuller's earth sample, showed that, up to 80 °C, a one-layer hydrate is stable (Bray et al. 1998). Waclawska (1984) found evidence of a second stage of dehydration. Firstly the water that forms the hydration layers is loosely bound in the structure of montmorillonite is removed, whereupon water forming the hydration sheaths of cations is released. This occurs when $\alpha = 0.8$, the second stage of dehydration accounting for loss of 20% of interlayer water. However, no mention has been made of reaction mechanisms and no calculations for the energetics of the final stage have been made (Waclawska 1984).

From the 'lnln' plots of the second stage of dehydration a diffusional process could describe the rate-limiting step. It is easy to envisage a two-dimension diffusion dominating mechanism, since this would describe the movement of water parallel to (001) from the interlayer to the reaction front.

Activation energies (E_a) determined for the first stage of dehydration using the Avrami, Austin-Rickett, Eq. (7) and integrated rate equations generate a range of values, from 28.6 kJ · mol⁻¹ to 40.6 kJ · mol⁻¹ (Table 3). The activation energy (E_a) determined from the "ln time to a give fraction method" (34.7 ± 0.9 kJ · mol⁻¹), fitting to Eq. (9) (34.2 kJ · mol⁻¹), and the Gualtieri integrated rate equation (35.4 kJ · mol⁻¹), are all very similar. This is a good indication that the activation energy for removal of the first interlayer water by a nucleation and growth process is around 35 kJ · mol⁻¹. The second, slower, diffusion controlled reaction process, at $\alpha > 0.8$, has a higher activation energy (E_a) of 47 ± 6 kJ · mol⁻¹ as determined from the "ln time to a given fraction" method.

Acknowledgements The authors are grateful for support from RBB R & D, who provided the sample of fuller's earth, and in particular to Dr Simon Drachman for his interest in the project. This work was supported by NERC in the form of studentship GT19/95/CS/2.

References

Annabli-Bergaya F, Estrade-Szwarczopf H, Van Damme H (1996) Dehydration of Cu-hectorite: water isotherm, XRD, and EPR studies. *J Phys Chem* 100: 4120–4126
 Austin JB, Rickett RL (1939) Kinetics of the decomposition of austenite at constant temperature. *Trans AIME* 135: 396–443

Avrami M (1939) Kinetics of phase change. I. General theory. *J Chem Phys* 7: 1103–1112
 Barker C (1972) Aquathermal pressuring – role of temperature in development of abnormal-pressure zones. *Am Assoc Petrol Geol Bull* 56: 2068–2071
 Bridgeman CH, Buckingham AD, Skipper NT, Payne MC (1996) Ab-initio total energy study of uncharged 2:1 clays and their interaction with water. *Mol Phys* 89: 879–888
 Bray HJ, Redfern SAT, Clark SM (1998) The kinetics of dehydration in Ca-montmorillonite: an in situ X-ray synchrotron study. *Mineral Mag* 62: 647–656
 Bruce CH (1984) Smectite dehydration – Its relation to structural development and hydrocarbon accumulation in northern Gulf of Mexico. *Am Assoc Petrol Geol Bull* 68: 673–683
 Burke J (1965) The kinetics of phase transformations in metals. Pergamon Press, Glasgow
 Burst JF (1969) Diagenesis of Gulf Coast clayey sediments and its possible relation to petroleum migration *Am Assoc Petrol Geol Bull* 53: 73–93
 Chang FRC, Skipper NT, Sposito G (1995) Computer simulation of interlayer molecular structure in sodium montmorillonite hydrates. *Langmuir* 11: 2734–2741
 Criado JM, Ortega A, Real C, Torres de Torres E (1984) Re-examination of the kinetics of the thermal dehydroxylation of kaolinite. *Clay Miner* 19: 653–661
 De Siqueira AVC, Skipper NT, Coveney PV, Boek ES (1997) Computer simulation evidence for enthalpy driven dehydration of smectite clays at elevated pressures and temperatures. *Mol Phys* 92: 1–6
 Eberl DD, Hower J (1976) Kinetics of illite formation. *Bull Geol Soc Am* 87: 1326–1330
 Farmer VC, Russell JD, (1967) IR absorption spectrometry in clay studies. *Clays Clay Miner* 15: 121–142
 Freed RL, Peacor DR (1989) Geopressured shale and sealing effect of smectite to illite transition. *Am Assoc Petrol Geol Bull* 73: 1223–1232
 Girgis BS, El-Barawy KA, Feli NS (1986) Dehydration kinetics of some smectites: a thermogravimetric study. *Thermochemica Acta* 98: 181–189
 Goss J (1987) The kinetics and reaction mechanism of the goethite to hematite transformation. *Mineral Mag* 51: 437–451
 Greene-Kelly R (1955) Dehydration of montmorillonite minerals. *Clay Minerals Bull* 5: 604–615
 Gualtieri A, Bellotto M, Artioli G, Clark SM (1995) Kinetic study of the kaolinite-mullite reaction sequence. Part II: mullite formation. *Phys Chem Minerals* 22: 215–222
 Güler C, Sarier N (1990) Kinetics of thermal dehydration of acid-activated montmorillonite by the rising temperature technique. *Thermochemica Acta* 159: 29–33
 Hancock JD, Sharp JH (1972) Method of comparing solid-state kinetic data and its application to the decomposition of kaolinite, brucite and BaCO₃. *J Am Ceram Soc* 55: 74–77
 Heller-Kallai L, Rozenson I (1980) Dehydroxylation of dioctahedral phyllosilicates. *Clays Clay Miner* 28: 355–368
 Howard J, Roy DM (1985) Development of layer charge and kinetics of experimental smectite alteration. *Clays Clay Miner* 33: 81–88
 Hower J, Eslinger E, Hower ME, Perry EA (1976) Mechanism of burial metamorphism of argillaceous sediment 1. Mineralogical and chemical evidence. *Geol Soc Am Bull* 86: 725–737
 Huang WL, Bassett WA, Wu T-C (1994) Dehydration and hydration of montmorillonite at elevated temperatures and pressures monitored using synchrotron radiation. *Am Mineral* 79: 683–691
 Karaborni S, Smit B, Urah J, van Oort E (1996) The swelling of clays: molecular simulations of the hydration of montmorillonite. *Science* 271: 1102–1104
 Koster van Groos AF, Guggenheim S (1984) The effect of pressure on the dehydration reaction of interlayer water in Na-montmorillonite. *Am Mineral* 69: 872–879
 Koster van Groos AF, Guggenheim S (1986) Dehydratoin of K-exchanged montmorillonite at elevated temperatures and pressures. *Clays Clay Miner* 34: 281–286

- Koster van Groos AF, Guggenheim S (1987) Dehydration of a Ca- and a Mg-exchanged montmorillonite (SWy-1) at elevated pressures. *Am Mineral* 72: 292–298
- Line CMB, Putnis A, Putnis C, Giampaolo C (1995) The dehydration kinetics and microtexture of analcime from two parageneses. *Am Mineral* 80: 268–279
- Low PF (1979) Nature and properties of water in montmorillonite-water systems. *Soil Sci Am J* 45: 651–658
- Magara K (1975) Reevaluation of montmorillonite dehydration as cause of abnormal pressure and hydrocarbon migration. *Am Assoc Petrol Geol Bull* 59: 292–302
- Miletich R, Zemann J, Nowak M (1997) Reversible hydration in synthetic mixite, $\text{BiCu}_6(\text{OH})_6(\text{AsO}_4)_3 \cdot n\text{H}_2\text{O}$ ($n < 3$): hydration kinetics and crystal chemistry. *Phys Chem Minerals* 24: 411–422
- Mohamed BM, Sharp JH (1997) Kinetics and mechanisms of formation of monocalcium aluminate, CaAl_2O_4 . *J Mat Sci* 7: 1595–1599
- Moore DM, Hower J (1986) Ordered interstratification of dehydrated and hydrated Na-smectite. *Clays Clay Miner* 34: 379–384
- Murray P, White J (1949) Kinetics of the thermal dehydration of clays. *Trans Brit Ceram Soc* 48: 187–206
- Murray P, White J (1955a) Kinetics of the thermal dehydration of clays. Part I. Dehydration characteristics of the clay minerals. *Trans Brit Ceram Soc* 54: 137–149
- Murray P, White J (1955b) Kinetics of the thermal dehydration of clays. Part II. Isothermal decomposition of the clay minerals. *Trans Brit Ceram Soc* 54: 151–187
- Murray P, White J (1955c) Kinetics of the thermal dehydration of clays. Part III. Kinetics analysis of mixtures of the clay minerals. *Trans Brit Ceram Soc* 54: 189–203
- Murray P, White J (1955d) Kinetics of the thermal dehydration of clays. Part IV. Interpretation of the differential thermal analysis of the clay minerals. *Trans Brit Ceram Soc* 54: 204–238
- Perry EA, Hower J (1972) Late-stage dehydration in deeply buried sediments. *Am Assoc Petrol Geol Bull* 56: 2013–2021
- Plumley WJ (1980) Abnormally high fluid pressure. Survey of some basic principles. *Am Assoc Petrol Geol Bull* 64: 414–430
- Powers MC (1967) Fluid-release mechanisms in compacting marine mudrocks and their importance in oil exploration. *Am Assoc Petrol Geol Bull* 51: 1240–1254
- Pytte AM, Reynolds RC (1988) The thermal transformations of smectite to illite. In: Vaeser ND, McCulloh TH, (eds.) *Thermal histories of sedimentary basins*. Springer Verlag, New York Berlin Heidelberg pp 133–140
- Ransom B, Helgeson HC (1995) A chemical and thermodynamic model of dioctahedral 2:1 layer clay minerals in diagenetic processes: dehydration of dioctahedral aluminous smectite as a function of temperature and depth in sedimentary basins. *Am J Sci* 295: 245–281
- Redfern SAT (1987) The kinetics of dehydroxylation of kaolinite. *Clay Miner* 22: 447–456
- Robertson HE, Lahann RW (1981) Smectite to illite conversion rates: effect of solution chemistry. *Clays Clay Miner* 29: 401–411
- Ruan HD, Gilkes RJ (1996) Kinetics of thermal dehydroxylation of aluminous goethite. *J Thermal Anal* 46: 1223–1238
- Sharp JH, Brindley GW, Narahari Achar BN (1966) Numerical data for some commonly used solid state reaction equations. *J Am Ceram Soc* 49: 379–382
- Skipper NT, Refson K, McConnell JDC (1989) Computer calculation of water-clay interactions using atomic pair potentials. *Clay Miner* 24: 411–425
- Skipper NT, Refson K, McConnell JDC (1991) Computer simulation of interlayer water in 2:1 clays. *J Chem Phys* 91: 7434–7445
- Skipper NT, Chang FRC, Sposito G (1995a) Monte Carlo simulation of interlayer molecular-structure in swelling clay minerals. 1. Methodology. *Clays Clay Miner* 43: 285–293
- Skipper NT, Sposito G, Chang FRC (1995b) Monte Carlo simulations of interlayer molecular-structure in swelling clay-minerals. 2. Monolayer hydrates. *Clays Clay Miner* 43: 294–303
- Tang L, Sparks DL (1993) Cation-exchange kinetics on montmorillonite using pressure-jump relaxation. *Soil Sci Am J* 57: 42–46
- Velde B, Vasseur G (1992) Estimation of the diagenetic smectite to illite transformation in time-temperature space. *Am Mineral* 77: 967–976
- Waclawska I (1984) Dehydration and dehydroxylation of smectites 1. Dehydration and dehydroxylation kinetics. *Mineral Polonica* 158: 91–107
- Weaver CE, Beck KC (1971) Clay water diagenesis during burial: how mud becomes gneiss. The Geological Society of America, Boulder, Colorado
- Wu T-C, Bassett WA, Huang W-L, Guggenheim S, Koster van Groos AF (1997) Montmorillonite under high H_2O pressure: stability of hydrate phases, rehydration hysteresis, and the effect of interlayer cation. *Am Mineral* 82: 69–78